Available online at www.sciencedirect.com
SCIENCE DIRECT®
Journal of Computational Physics 202 (2005) 52–64
JOURNAL OF COMPUTATIONAL PHYSICS
www.elsevier.com/locate/jcp

The method of series expansion for 3-D vector tomography reconstruction

A.L. Balandin [a,*], Y. Ono [b]

[a] Institute of Systems Dynamics and Control Theory, Lermontov str. 134, 664033, Irkutsk-33, Russia
[b] High Temperature Plasma Center, University of Tokyo, 2-11-16 Yayoi, Bunkyo-ku, Tokyo 113-8656, Japan

Received 27 September 2003; received in revised form 1 July 2004; accepted 1 July 2004
Available online 21 August 2004

Abstract

The method of series expansion has been developed for the inversion of the X-ray transform of three-dimensional (3-D) vector fields, and the corresponding vector central-slice theorem derived. The simulation demonstrating the 3-D reconstruction of the model vector fields is presented.

Keywords: Inverse problems; Computerized tomography; Spherical harmonics

1. Introduction

Recent years have given evidence of growing necessity to apply tomography reconstruction techniques to flow diagnostics. In many physical experiments the number of two-dimensional (2-D) measurements is usually executed by collecting a line of sight information, which is essentially integral. In case of scalar objects, the 2-D measured data are the projections of 3-D density. In more complex models, like plasma, the spectroscopic measurements, for example, can contain both information concerning the distribution of parameters of scalar and vector (velocity) fields. The majority of works on vector tomography have been dedicated to the Radon transform [1–4]. Norton [1] have derived the central-slice theorem for a 2-D vector field and shown that only the solenoidal (divergent-free) component of the field can be reconstructed from the time-of-flight measurements. Braun and Hauck [2] have shown that usage of

* Corresponding author. Fax: +81 7 3952 511616.
E-mail addresses: balandin@icc.ru (A.L. Balandin), ono@ts.t.u-tokyo.ac.jp (Y. Ono).

0021-9991/$ - see front matter © 2004 Published by Elsevier Inc.
doi:10.1016/j.jcp.2004.07.001

"longitudinal" and "transversal" interaction effect allows one to perform complete reconstruction of a vector field. Prince [3] has developed the backprojection algorithm for the 3-D vector field and shown that irrotational and solenoidal components of the field, in principle, can be recovered separately by using probe measurements.

The method of series expansion for scalar fields has been investigated by several authors. Mijnarends [5] has solved the reconstruction problem for 1-D projection data in an object space. The solution for the 2-D projection data has been for the first time given by Majumdar [6], as well as by Wang and Granetz [8] for an object space. Pecora [7] has developed the inversion method for 2-D projection data in Fourier space. Wang [10] has proposed the analytical inversion formula for the X-ray transform in 3-D space.

In many experiments, the reconstruction problem is hard to be solved since it is often experimentally impossible to obtain more than a few projections of the object. In this paper, a numerical method is proposed for the inversion of the X-ray transform of 3-D vector fields, which is based on the method of series expansion, which is often preferred by physicists and is quite appropriate for real experimental measurements.

The left-hand side of Eq. (2) is obtained as the inner product of the vector field and the unit vector $\boldsymbol{\chi}$. In case of spectroscopic measurements, in the process of plasma experiments, the vector $\boldsymbol{\chi}(\mathbf{n})$ merely coincides with the vector $\mathbf{n}$ which is determined by the line of observation [11].

The object coordinate system, $S' = (\mathbf{e}'_1,\mathbf{e}'_2,\mathbf{e}'_3)$, with the coordinates $\mathbf{x}' = (x',y',z')$ will, in general, be rotated with respect to the laboratory frame of reference, $S = (\mathbf{e}_1,\mathbf{e}_2,\mathbf{e}_3)$, with the coordinates $\mathbf{x} = (x,y,z)$. The laboratory coordinate system S is assumed to be related to the measurement coordinate system with the axis z along the line of observation and is fixed throughout the experiment. The rotations are considered as active transformations, i.e., rotation of a vector (object) in a fixed coordinate frame [1] [12]. The rotation matrix $R(\alpha,\beta,\gamma)$ mapping any vector $\mathbf{x}$ into a new vector $\mathbf{x}'$ by the formula

$$\mathbf{x}' = R(\alpha,\beta,\gamma)\mathbf{x}. \tag{1}$$

The Euler angles (α,β,γ) are likewise defined in [13]. The angles β and α are, respectively, the polar and the azimuth angles of the axis z' referred to the system of reference S. For the positive Euler angles (α,β,γ) the rotation matrix is as follows [2]

$$R = \left(\begin{array}{c|c|c} \cos\alpha\cos\beta\cos\gamma - \sin\alpha\sin\gamma & -\cos\alpha\cos\beta\sin\gamma - \sin\alpha\cos\gamma & \cos\alpha\sin\beta \\ \sin\alpha\cos\beta\cos\gamma + \cos\alpha\sin\gamma & -\sin\alpha\cos\beta\sin\gamma + \cos\alpha\cos\gamma & \sin\alpha\sin\beta \\ -\sin\beta\cos\gamma & \sin\beta\sin\gamma & \cos\beta \end{array}\right),$$

$$0 \le \alpha < 2\pi,\ 0 \le \beta \le \pi,\ 0 \le \gamma < 2\pi.$$

The tomographic reconstruction of the 3-D vector field in the paper has been performed in terms of spherical harmonics from a relatively small number of 2-D data sets. Test examples using objects of some spherical symmetry and/or band-limited with respect to angular variables show that reconstruction can work well when small number of directions are available. A band-limited function can be computed exactly by finite sums of sampled values of this function on the sphere [14].

Below, in Section 2, we first of all discuss the Central Slice Theorem for the vector X-ray transform. Section 3 describes the inversion method. The results of the computer simulation are given in Section 4. Some useful properties of Wigner D-functions employed in the computations are given in Appendix A.

[1] In contrast, passive rotation is rotation of the coordinate system.

[2] For the positive angle the rotation appears counterclockwise with respect to an observer looking towards the origin.

2. The central slice theorem

In this section, the Central Slice Theorem for the vector X-ray transform is derived, and, as the corollary it is obtained that the irrotational component of the vector field gives no contribution to the path-integral Eq. (2), leaving only the contribution from the solenoidal part. Although the vector X-ray transform is different from the vector Radon transform in 3-D space, the result obtained is quite similar for both cases [1,3].

The X-ray transform of the 3-D vector field $\mathbf{g}(\mathbf{x})$ is defined as follows:

$$(\mathcal{X}\mathbf{g})(\mathbf{x},\mathbf{n}) \equiv f(\mathbf{x},\mathbf{n}) = \int_{-\infty}^{\infty} \mathbf{g}(\mathbf{x}+t\mathbf{n})\cdot\boldsymbol{\chi}(\mathbf{n})\,\mathrm{d}t, \quad \mathbf{x}\in\mathbf{n}^{\perp}. \tag{2}$$

The vector field $\mathbf{g}(\mathbf{x})$ is assumed to be defined on the Schwartz class of rapidly decreasing $\mathbb{C}^{\infty}$ functions on $\mathbb{R}^3, \mathbf{g}(\mathbf{x}) \in \mathbb{S}(\mathbb{R}^3,\mathbb{R}^3)$. The vector function $\boldsymbol{\chi}$ is the one converting the vector field $\mathbf{g}$ into a scalar field by the inner product. As usually, $\mathbf{n}^{\perp}$ denotes the plane perpendicular to the vector $\mathbf{n}$. When we regard the vector $\mathbf{k}\in\mathbf{n}^{\perp}$ as a two dimensional one in the coordinates of $\mathbf{n}^{\perp}$, we denote it by $\mathbf{k}_{\perp}$ for distinction. Taking the 2-D Fourier transform for both sides of (2) over $\mathbf{x}$-variable, as a result of computations, we obtain the following formula which is a vector version of the Central Slice Theorem (cf. [15] for the scalar case):

$$\mathcal{F}_2 f(\mathbf{k}_{\perp},\mathbf{n}) = \boldsymbol{\chi}(\mathbf{n})\cdot\mathcal{F}_3\mathbf{g}(\mathbf{k}), \quad \mathbf{k}\in\mathbf{n}^{\perp}, \tag{3}$$

where $\mathcal{F}_2$ and $\mathcal{F}_3$ denote 2-D and 3-D direct Fourier transforms, respectively. According to Helmholtz's decomposition theorem [16], any vector field $\mathbf{g}(\mathbf{x})$ can, with a suitable regularity, be uniquely written as the sum of the irrotational and the solenoidal components

$$\mathbf{g} = \mathbf{g}_{\mathrm{i}} + \mathbf{g}_{\mathrm{s}}, \quad \mathbf{g}_{\mathrm{i}} = \nabla\varphi, \quad \mathbf{g}_{\mathrm{s}} = \nabla\times\boldsymbol{\psi}, \tag{4}$$

where φ and $\boldsymbol{\psi}$ are scalar and vector potentials, respectively. The 3-D Fourier transforms of the irrotational and solenoidal components of $\mathbf{g}$ are

$$\mathcal{F}_3\mathbf{g}_{\mathrm{i}} = \mathrm{i}\mathbf{k}\mathcal{F}_3\varphi(\mathbf{k}), \quad \mathcal{F}_3\mathbf{g}_{\mathrm{s}} = \mathrm{i}\mathbf{k}\times\mathcal{F}_3\boldsymbol{\psi}(\mathbf{k}). \tag{5}$$

The formula Eq. (3) can now be rewritten in the form

$$\mathcal{F}_2 f(\mathbf{k}_{\perp},\mathbf{n}) = \mathrm{i}\boldsymbol{\chi}(\mathbf{n})\cdot\mathbf{k}_{\perp}\mathcal{F}_3\varphi(\mathbf{k}) + \mathrm{i}\boldsymbol{\chi}(\mathbf{n})\cdot(\mathbf{k}\times\mathcal{F}_3\boldsymbol{\psi}(\mathbf{k})), \tag{6}$$

where $\mathbf{k}\in\mathbf{n}^{\perp}$, i.e., the 3-D vector $\mathbf{k}$, lies in the plane $\mathbf{n}^{\perp}$. If $\boldsymbol{\chi}(\mathbf{n}) = \mathbf{n}$ (as we assume from now on) then the first summand of (6) is zero and, therefore, there is no contribution of the irrotational component to the projection data. The following equality takes a place

$$\mathcal{F}_2 f(\mathbf{k}_{\perp},\mathbf{n}) = \mathbf{n}\cdot\mathcal{F}_3\mathbf{g}_s(\mathbf{k}), \quad \mathbf{k}\in\mathbf{n}^{\perp}. \tag{7}$$

As follows from (7), only information on the solenoidal component of the vector field is present in the experimental data.

3. The inversion method

The main problem of inversion is to choose such a representation of the rotation group that, when the vector field $\mathbf{g}(\mathbf{x})$ is expanded in terms of some basis functions, its X-ray transform is expanded in terms of the same basis functions. Whereas the solenoidal component of the field can be recovered from integral measurement data, the scalar potential φ and, consequently, the irrotational part $\mathbf{g}_{\mathrm{i}}(\mathbf{x})$ of the field under the constraint $\operatorname{div}\mathbf{g} = 0$ can be found as a solution of Laplace's equation with the values of $\mathbf{g}$ on the boundary. To wit, the irrotational component can independently be recovered [1].

Henceforth, due to (7), we will deal only with the solenoidal component $\mathbf{g}_s(\mathbf{x})$ of any vector field, and for simplicity we willll use the notation $\mathbf{g}(\mathbf{x})$ for $\mathbf{g}_s(\mathbf{x})$.

Any vector field in its own coordinate system (S') is decomposed as follows:

$$\mathbf{g}(\mathbf{x}') = \sum_{i=1}^{3} g_i(\mathbf{x}')\mathbf{e}'_i. \tag{8}$$

Similarly to (1), the functions $g_i(\mathbf{x}')$ can be represented in the laboratory frame S by using an operator $\mathcal{R}$ which transforms scalar functions from the object coordinate system S' to the laboratory frame. Thus, in the laboratory frame $\mathcal{R}g_i(\mathbf{x})$, are the functions representing the object (components of the field). Since $g_i(\mathbf{x}')$ are scalar functions the following equality takes place

$$\mathcal{R}g_i(R^{-1}\mathbf{x}') = g_i(\mathbf{x}'). \tag{9}$$

Now choose the rotation so that the line of integration representing the projections (X-ray transform) taking place in the experiment be directed along the axis z in the laboratory frame. Then, the equation for the data writes

$$\breve{g}(p,\alpha,\beta,\gamma) = \int_{L(p,\alpha,\beta,\gamma)} \mathbf{g}(\mathbf{x}')\,\mathrm{d}\mathbf{l}' = \sum_{i=1}^{3} \int_{L(p,\alpha,\beta,\gamma)} g_i(\mathbf{x}')\mathbf{e}'_i\,\mathrm{d}\mathbf{l}' \quad = \sum_{i=1}^{3} \int_{-\infty}^{\infty} \mathcal{R}g_i(R^{-1}\mathbf{x}')n_i\,\mathrm{d}z, \tag{10}$$

here n_i is ith component of the vector $\mathbf{n} = (\cos\alpha\sin\beta, \sin\alpha\sin\beta, \cos\beta)$.

The Euler angles (α,β,γ) and the integration path $L(p,\alpha,\beta,\gamma)$ are shown in Fig. 1. The variable p is measured along of the axis x from the origin.

Under general conditions, any scalar function $g_i(\mathbf{x}')$ can be expanded in the series of spherical harmonics $Y_{l\,m}(\theta',\varphi')$ and hence operator $\mathcal{R}$ is specified as follows:

$$g_i(\mathbf{x}') = \mathcal{R}g_i(R^{-1}\mathbf{x}') = \sum_{n=0}^{\infty}\sum_{l=0}^{\infty}\sum_{m=-l}^{l} C^i_{lmn}Y_{lm}(\theta',\varphi')f_{ln}(r), \tag{11}$$

where θ' and φ' are polar and azimuthal angles of the point $\mathbf{x}'$ in an object coordinate system S', C^i_{lmn} are complex coefficients, the orthogonal polynomials $f_{ln}(r)$ is defined below. The spherical harmonics $Y_{lm}(\theta,\varphi)$ are given as follows

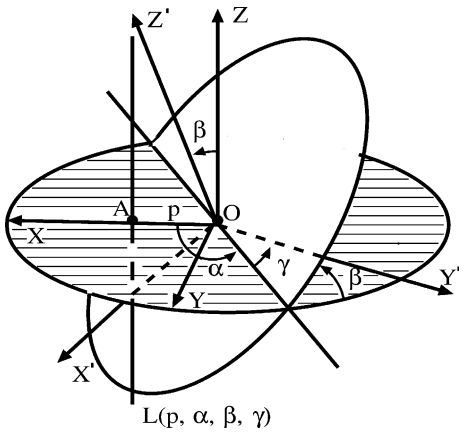

Fig. 1. The integration path $L(p,\alpha,\beta,\gamma)$ and Euler angles for the X-ray transform. XYZ and $X'Y'Z'$ are the laboratory and the object coordinate systems, respectively. Integration is always performed along the axis Z with different α, β, γ, p = OA.

$$Y_{lm}(\theta,\varphi) = (-1)^m \left(\frac{(2l+1)(l-m)!}{4\pi(l+m)!}\right)^{1/2} P_l^m(\cos\theta)\ \exp(\mathrm{i}m\varphi),$$

where $P_l^m(\cos\theta)$ are associated Legendre functions.

Under rotation, characterized by Euler's angles (α,β,γ), the spherical harmonics Y_{lm} are transformed according to the formula

$$Y_{lm}(\theta',\varphi') = \sum_{m'=-l}^{l} D^l_{m'm}(\alpha,\beta,\gamma) Y_{lm'}(\theta,\varphi), \tag{12}$$

where (θ',φ') are spherical coordinates in the object coordinate system S', whereas (θ,φ) are the coordinates in the laboratory system S. Based on the property (12) the components $g_i(\mathbf{x}')$ are rewritten in an invariant form

$$g_i(\mathbf{x}') = \mathcal{R} g_i(R^{-1}\mathbf{x}') = \sum_{n=0}^{\infty}\sum_{l=0}^{\infty}\sum_{m=-l}^{l}\sum_{m'=-l}^{l} C^i_{lmn} D^l_{m'm}(\alpha,\beta,\gamma) Y_{lm'}(\theta,\varphi) f_{ln}(r). \tag{13}$$

The function $\breve{g}(p,\alpha,\beta,\gamma)$ now writes

$$\breve{g}(p,\alpha,\beta,\gamma) = \sum_{l,m,n,i} C^i_{lmn} \sum_{m'} D^l_{m'm}(\alpha,\beta,\gamma) n_i \int_{-\infty}^{\infty} Y_{lm'}(\theta,\varphi) f_{ln}(r)\,\mathrm{d}z, \tag{14}$$

or, by an equivalent relation with the real coefficients A^i_{lmn}, B^i_{lmn} [9],

$$\breve{g}(p,\alpha,\beta,\gamma) = \sum_{n=0}^{\infty}\sum_{l=0}^{\infty}\sum_{m=0}^{l}\sum_{i=1}^{3} [A^i_{lmn} W_{lmn} + B^i_{lmn} V_{lmn}] n_i, \tag{15}$$

where the functions W_{lmn} and V_{lmn} are, respectively,

$$W_{lmn} \equiv W_{lmn}(p,\alpha,\beta,\gamma) = \int_{-\infty}^{\infty} \mathrm{d}z S^c_{lm}(\theta,\varphi) f_{ln}(r) = \sum_{k=0}^{l} \mathcal{W}_{lmk}(\alpha,\beta,\gamma) u_{lkn}(p), \tag{16}$$

$$V_{lmn} \equiv V_{lmn}(p,\alpha,\beta,\gamma) = \int_{-\infty}^{\infty} \mathrm{d}z S^s_{lm}(\theta,\varphi) f_{ln}(r) = \sum_{k=0}^{l} \mathcal{V}_{lmk}(\alpha,\beta,\gamma) u_{lkn}(p). \tag{17}$$

The functions $\mathcal{W}_{lmk}$ and $\mathcal{V}_{lmk}$ are obtained as a result of separation of the Wigner's D-function and spherical harmonics Y_{lm} into the real and the imaginary parts.

$$\mathcal{W}_{lmk}(\alpha,\beta,\gamma) = \delta_k[\cos(m\alpha + k\gamma) d^l_{mk}(\beta) + (-1)^k \cos(m\alpha - k\gamma) d^l_{m,-k}(\beta)],$$
$$\mathcal{V}_{lmk}(\alpha,\beta,\gamma) = \delta_k[\sin(m\alpha + k\gamma) d^l_{mk}(\beta) + (-1)^k \sin(m\alpha - k\gamma) d^l_{m,-k}(\beta)],$$
$$\delta_0 = 0.5 \text{ and } \delta_k = 1 \text{ if } k \neq 0.$$

The definition and some properties useful for numerical computation of D-functions and functions $d^l_{mk}(\beta)$ are given in Appendix A.

The real spherical harmonics S^c_{lm} and S^s_{lm} are defined as

$$S^c_{lm}(\theta,\varphi) = \frac{Y_{lm}(\theta,\varphi) + Y^*_{lm}(\theta,\varphi)}{2}, \quad S^s_{lm}(\theta,\varphi) = \frac{Y_{lm}(\theta,\varphi) - Y^*_{lm}(\theta,\varphi)}{2i}. \tag{18}$$

If the orthogonal polynomials $f_{ln}(r)$ are chosen to be of the following form:

$$f_{ln}(r) = r^l(1-r^2) P_n^{(l+1/2,1)}(1-2r^2), \tag{19}$$

then the functions $u_{lmn}(p)$ can be represented analytically [9,10]:

$$u_{lmn}(p) = \begin{cases} \mathcal{C}_{lmn} p^m (1-p^2)^{3/2} P^{(m,3/2)}_{(l-m)/2+n}(1-2p^2), & l+m = \text{even}, \\ 0, & l+m = \text{odd}. \end{cases} \tag{20}$$

The constants $\mathcal{C}_{lmn}$ are equal to

$$\mathcal{C}_{lmn} = \frac{(-1)^l (n+1)((l-m)/2+n)!\{(2l+1)(l-m)!(l+m)!\}^{1/2}}{2^{l+1}\Gamma((l-m)/2+n+5/2)((l-m)/2)!((l+m)/2)!}.$$

The Jacobi polynomials $P_n^{(\alpha,\beta)}(x)$, which occurred in (19) and (20) can be evaluated with the aid of Gauss' hypergeometric function [19]:

$$P_n^{(\alpha,\beta)}(x) = \frac{\Gamma(n+1+\alpha)}{n!\Gamma(1+\alpha)} {}_2F_1\left(n+\alpha+\beta+1, -n; 1+\alpha; \frac{1-x}{2}\right). \tag{21}$$

The series in (21) break off, and polynomials $P_n^{(\alpha,\beta)}(x)$ are calculated efficiently.

For the purpose of numerical confirmation of the fact that formula (10) can be represented by formulas (15)–(17), we give Fig. 2, which shows two curves of the function $\breve{g}(p,\alpha,\beta,\gamma)$ with respect to the variable p with some fixed values of angles (α,β,γ). The computations are performed by formula (10) (thick line) and by formulas (15)–(17) (thin line). The coincidence of the curves is explicit.

The number of series expansion terms in Eq. (15) is infinite, however, in practical calculations the number of measured data is finite, therefore the series has to be truncated. Eq. (15) after truncation as below is solved with respect to the variables A^i_{lmn}, B^i_{lmn} by the least squares method [18]. The values A^i_{lmn} and B^i_{lmn} are obtained as a result of minimization of the functional Φ, the sum of squares of the differences between the experimental values of $\breve{g}(p,\alpha,\beta,\gamma)$ and the computed ones:

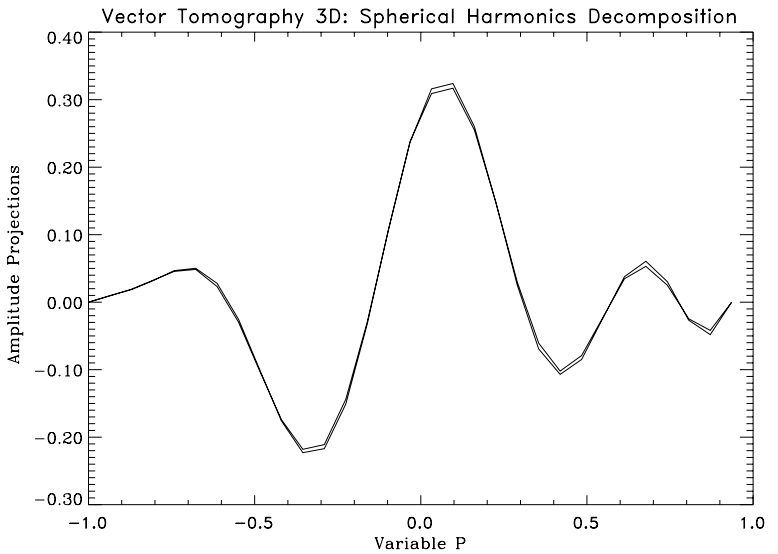

Fig. 2. The projections $\breve{g}(p,\alpha,\beta,\gamma)$ have been computed numerically by the formula (10) (thick line) and by the formulas (15)–(17) (thin one), respectively, for the fixed values of the angles (α, β, γ).

$$\Phi = \int_0^\infty \mathrm{d}p \int \mathrm{d}R \left\{ \breve{g}(p,\alpha,\beta,\gamma) - \sum_{l=0}^{L} \sum_{m=0}^{l} \sum_{n=0}^{N} \sum_{i=1}^{3} \left[A^i_{lmn} W_{lmn} + B^i_{lmn} V_{lmn} \right] n_i \right\}^2, \tag{22}$$

where R will henceforth denote the Euler angles (α, β,γ), and we also will set $\mathrm{d}R = \sin\beta\,\mathrm{d}\beta\,\mathrm{d}\alpha\,\mathrm{d}\gamma$:

$$\int \mathrm{d}R f(R) = \int_0^{2\pi} \mathrm{d}\alpha \int_0^{\pi} \sin\beta\,\mathrm{d}\beta \int_0^{2\pi} \mathrm{d}\gamma f(\alpha,\beta,\gamma).$$

The equations

$$\left(\partial\Phi/\partial A^i_{l'm'n'}\right) = 0, \left(\partial\Phi/\partial B^i_{l'm'n'}\right) = 0, \tag{23}$$

are linear in A^i_{lmn} and B^i_{lmn} for each (l,m,n) and i = 1,2,3 and can be written as follows:

$$\sum_{\nu=1}^{\mathcal{N}} \mathcal{A}_{\mu\nu} X_\nu = Y_\mu. \tag{24}$$

In actual computations, the column vectors X_ν and Y_μ each have $\mathcal{N} = 3N(L+1)^2$ components, and the square matrix $\mathcal{A}_{\mu\nu}$ has $\mathcal{N}^2$ components of which at most $(\mathcal{N}+1)\mathcal{N}/2$ components are different,

$$\mathcal{A}_{\mu\nu} = \begin{cases} W^i_{lmn} W^j_{l'm'n'}, \\ \text{when} \begin{cases} \mu = (L+1)^2((i-1)N + (n-1)) + l^2 + m, \\ \nu = (L+1)^2((j-1)N + (n'-1)) + l'^2 + m', \end{cases} \\ W^i_{lmn} V^j_{l'm'n'}, \\ \text{when} \begin{cases} \mu = (L+1)^2((i-1)N + (n-1)) + l^2 + m, \\ \nu = (L+1)^2((j-1)N + (n'-1)) + l'^2 + l' + m', \quad m' \neq 0, \end{cases} \\ V^i_{lmn} W^j_{l'm'n'}, \\ \text{when} \begin{cases} \mu = (L+1)^2((i-1)N + (n-1)) + l^2 + l + m, \quad m \neq 0, \\ \nu = (L+1)^2((j-1)N + (n'-1)) + l'^2 + m', \end{cases} \\ V^i_{lmn} V^j_{l'm'n'}, \\ \text{when} \begin{cases} \mu = (L+1)^2((i-1)N + (n-1)) + l^2 + l + m, \quad m \neq 0, \\ \nu = (L+1)^2((j-1)N + (n'-1)) + l'^2 + l' + m', \quad m' \neq 0. \end{cases} \end{cases}$$

Here $N = \max(n)$ is the maximum index for the radial component, L is the maximum number for the index l, i, j = 1, 2, 3. The case of i = 1 and j = 1 corresponds to the matrix for reconstruction of the scalar field. The solution of Eq. (24) gives the required values of the unknowns A^i_{lmn}, B^i_{lmn}. Then, after their substitution into Eqs. (8), (11), the problem is solved.

$$X_\nu = \begin{cases} A^i_{lmn}, \\ \text{when } \nu = (L+1)^2((i-1)N + (n-1)) + l^2 + m, \\ B^i_{lmn}, \\ \text{when } \nu = (L+1)^2((i-1)N + (n-1)) + l^2 + l + m, \quad m \neq 0, \end{cases}$$

$$Y_\mu = \begin{cases} \int_0^\infty \mathrm{d}p \int \mathrm{d}R\, \breve{g}(p,\alpha,\beta,\gamma) W^i_{l'm',n'}(p,\alpha,\beta,\gamma), \\ \text{when } \mu = (L+1)^2((i-1)N + (n'-1)) + l'^2 + m', \\ \int_0^\infty \mathrm{d}p \int \mathrm{d}R\, \breve{g}(p,\alpha,\beta,\gamma) V^i_{l'm',n'}(p,\alpha,\beta,\gamma), \\ \text{when } \mu = (L+1)^2((i-1)N + (n'-1)) + l'^2 + l' + m', \quad m' \neq 0. \end{cases}$$

4. Computer simulation

To illustrate the method, consider below the two models of the vector reconstruction problem. The first model is taken in the form (25) with $L = 3$ and with the following coefficients A^i_{lmn} and B^i_{lmn}:

$$g_i(\mathbf{x}') = \sum_{l=0}^{L} \sum_{m=0}^{l} \sum_{n=0}^{1} (A^i_{lmn} S^c_{lm}(\theta', \varphi') + B^i_{lmn} S^s_{lm}(\theta', \varphi')) f_{ln}(r), \quad i = 1,2,3, \tag{25}$$

$$A^1_{lmn} = \begin{cases} 1, \\ 0.5, \quad \text{if } l, m = 0, \end{cases} \quad B^1_{lmn} = \{-1, \quad \text{if } l, m \neq 0, \quad A^2_{lmn} = \begin{cases} 1, \\ 0.1, \quad \text{if } l, m = 0, \end{cases}$$

$$B^2_{lmn} = \{-0.1, \quad \text{if } l, m \neq 0, \quad A^3_{lmn} = \begin{cases} 0.5 \\ 0.2, \quad \text{if } l, m = 0, \end{cases} \quad B^3_{lmn} = \{-0.5, \quad \text{if } l, m \neq 0.$$

In the capacity of the second model the solenoidal field (div $\mathbf{g}(\mathbf{x}) = 0$) of the following form has been taken:

$$\mathbf{g}(\mathbf{x}') = \left(c_1 y' z' \exp\left(-\frac{r^2}{2a^2}\right), \; -c_2 x' z' \exp\left(-\frac{r^2}{2a^2}\right), \; c_3 \exp\left(-\frac{r^2 \sin^2\theta}{2b^2}\right) \right), \tag{26}$$

where $r^2 = x'^2 + y'^2 + z'^2$, $a = 0.3$, $b = 0.3$, $c_1 = 8.0$, $c_2 = 8.0$, $c_3 = 0.25$.

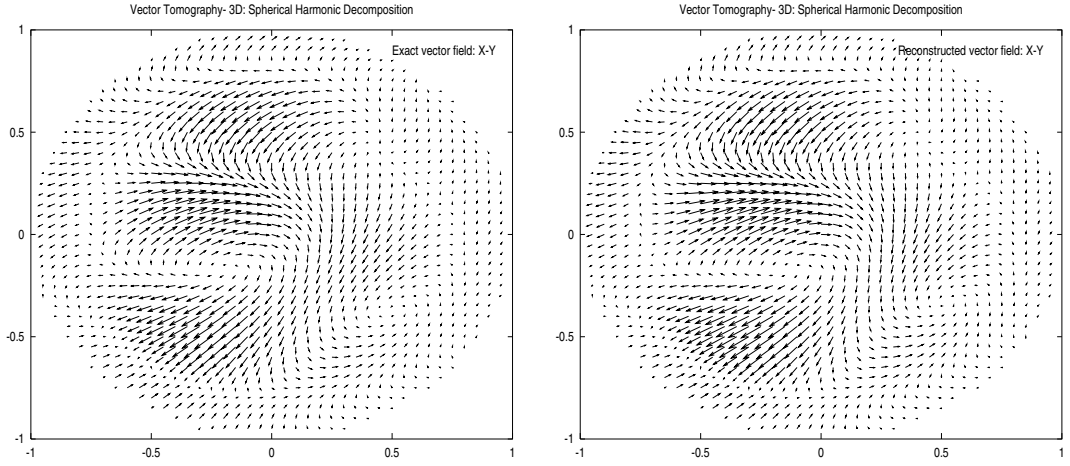

Fig. 3. Model one: precision (left) and reconstructed (right) vector fields on the plane $Z = 0$, $L = 3$.

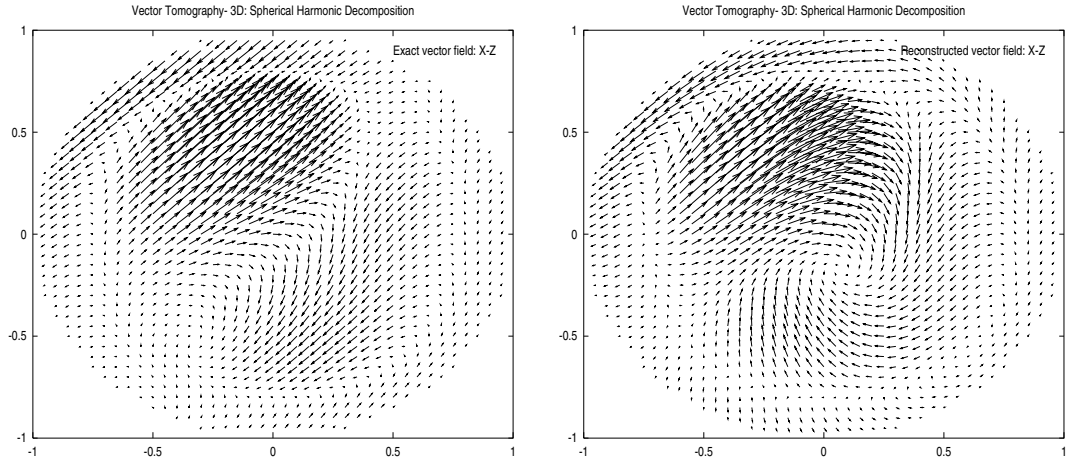

Fig. 4. Model one: precision (left) and reconstructed (right) vector fields on the plane $Y = 0$, $L = 3$.

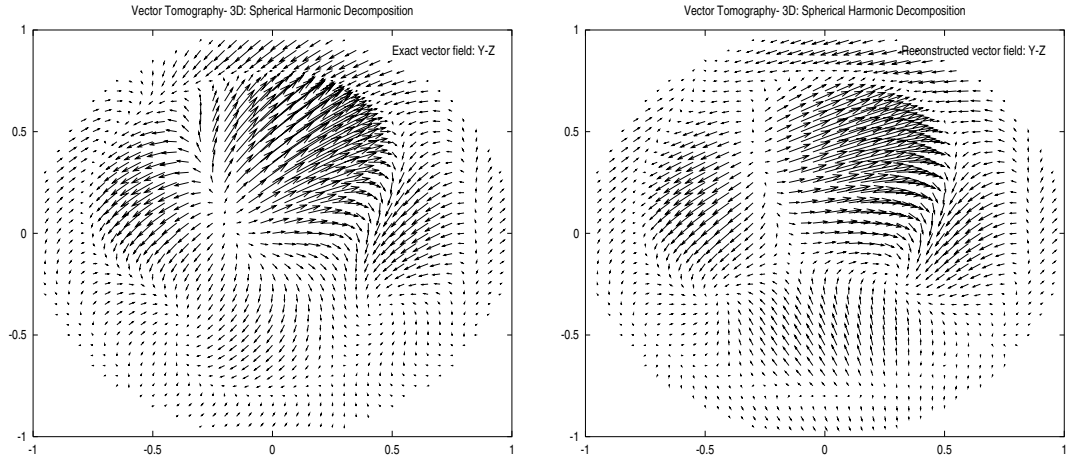

Fig. 5. Model one: precision (left) and reconstructed (right) vector fields on the plane $X = 0$, $L = 3$.

As the first model is described by the finite number of harmonics $(L + 1)^2$, the second one does contain an infinite number of spherical harmonics. All reconstructions were performed with the projection data spoiled by some artificial noise. The noise level was taken to be 5% of the maximum level of measured data (projections). The sum over l in (25) is restricted by $L = 3$ for the first model and by $L = 5$ for the second one. If the samples over angular variables are approximately equally spaced, the Nyquist principle can be used to estimate the maximum number of L and the maximum number of expansion harmonics that may be resolved. If however, this does not take place the Akaike information criterion (AIC) is often used in plasma diagnostic experiments [20]. In our spherical tokamak experiments large scale motion is considered, so the value of L is probably not larger than 5.

Sections of the 3-D model vector field and its reconstructions on the planes $Z = 0$, $Y = 0$, $X = 0$ are shown in Figs. 3–5 for the first and on Figs. 6–8 for the second models, respectively. The reconstruction

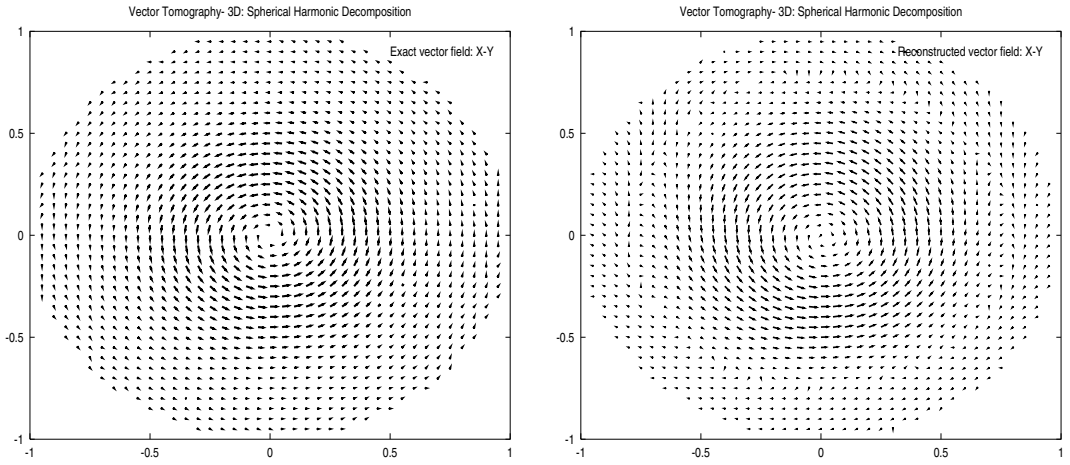

Fig. 6. Model two: precision (left) and reconstructed (right) vector fields on the plane $Z = 0$.

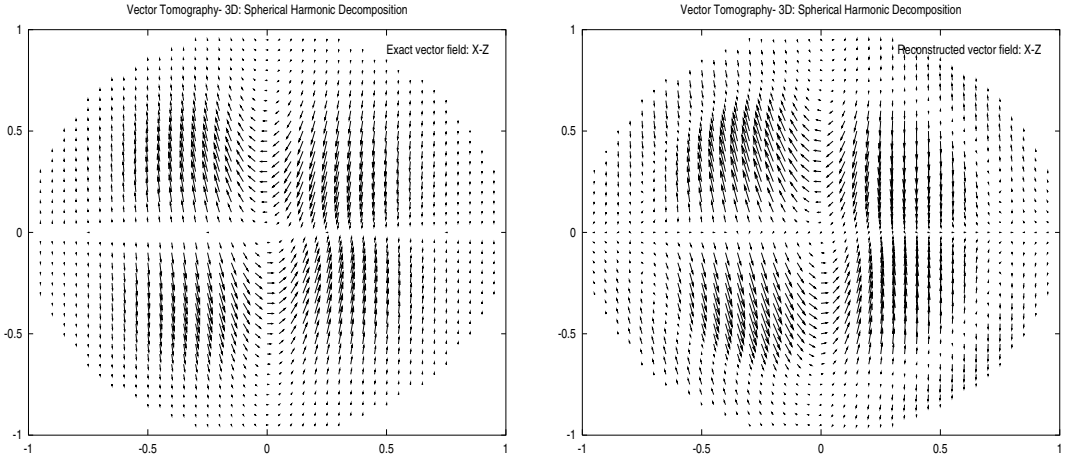

Fig. 7. Model two: precision (left) and reconstructed (right) vector fields on the plane $Y = 0$.

of the models is performed with a number of grid points $N_\alpha = 5$, $N_\beta = 5$, $N_\gamma = 4$, $N_p = 31$ for the variables (α,β,γ) and p, respectively.

In course of rotation of the object's coordinate system, the integration path $L(p,\alpha,\beta,\gamma)$ in Eq. (10) stays always along the axis Z while $Y = 0$, and X is varying from -1 to 1. Fig. 9 illustrates stability of the iterative procedure of solving Eq. (24). For the first model with $L = 5$ only the lower first 36 coefficients $A^1_{lm0} = 1, A^1_{000} = 0.5$ and $B^1_{lm0} = -1$ are taken nonzero, any other coefficients are put zero. The thick line shows the exact values of X_v, the thin line – computed values of X_v with $N_\alpha = 5$, $N_\beta = 5$, $N_\gamma = 4$, $N_p = 3$, and the "– · – · –" line shows the computed values with $N_\alpha = 8$, $N_\beta = 10$, $N_\gamma = 8$, $N_p = 31$. It can readily be seen that the relative error of reconstruction of the coefficients A^i_{lmn} and B^i_{lmn} is quite acceptable and substantially decreases with an increase in the number of projections.

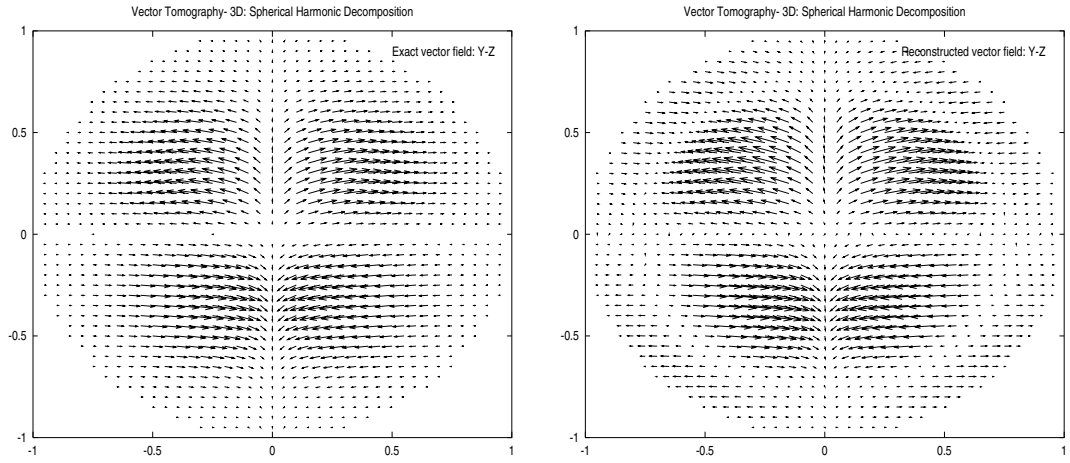

Fig. 8. Model two: precision (left) and reconstructed (right) vector fields on the plane $X = 0$.

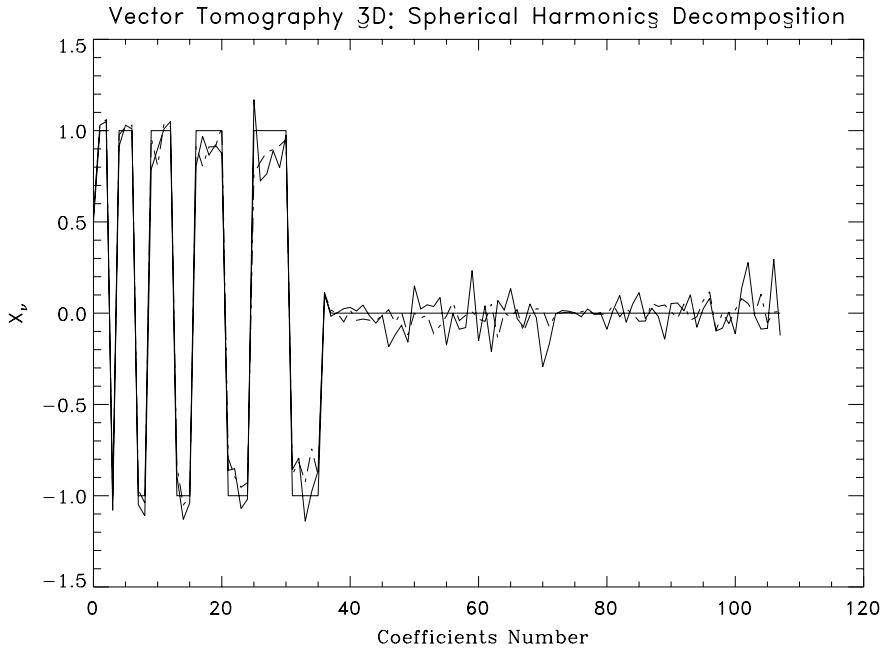

Fig. 9. Exact values of X_ν for the first model with $L = 5$ are depicted by thick line; the values of X_ν are obtained as the solutions of Eq. (24) with $N_\alpha = 5$, $N_\beta = 5$, $N_\gamma = 4$, $N_p = 31$ and with $N_\alpha = 8$, $N_\beta = 10$, $N_\gamma = 8$, $N_p = 31$ are drawn by the thin line and by the "– · – · –" line, respectively.

5. Conclusion

In this paper, we have investigated the problem of reconstructing a 3-D vector field using the line integrated data. The expansion of components of the vector field into the orthogonal system of spherical harmonics and then solving the linear system of equations with respect to expansion coefficients is an

important key to the analysis. This approach allows one to take an easy account of the shadow effect conditioned by the central coils in any spherical tokamak experiments.

In our approach, the matrix $\mathcal{A}_{\mu\nu}$ is diagonally dominant, what, on the one hand, provides stability of the algorithm, and on the other, the incomplete diagonality indicates that the components of the vector field intermix under rotation. In other words, another decomposition of the vector field probably exists.

In three dimensions, the vector potential $\boldsymbol{\psi}$ in (4) actually, unlike that in the two-dimensional case, when only one component of the vector potential exists, has three components. So, the vector potential formulation cannot be applied with essential advantage to the 3-D field in contrast to the 2-D case [1,11]. If the object of reconstruction is known to have some symmetry, which is often the case in spherical tokamak experiments, the truncation problem in (15) is simplified.

Acknowledgements

The first author thanks Prof. Makoto Katsurai and the staff of High-Temperature Plasma Center, University of Tokyo, for their hospitality.

Appendix A. Some properties of the Wigner D-functions

The matrix $D^J_{M_1M_2}(\alpha,\beta,\gamma)$ is a representation of *the group of rotations* SO(3) and is usually represented as a product of three functions, each depending on only one Euler angle (α,β,γ):

$$D^J_{M_1M_2}(\alpha,\beta,\gamma) = \mathrm{e}^{-\mathrm{i}M_1\alpha}\, d^J_{M_1M_2}(\beta)\mathrm{e}^{-\mathrm{i}M_2\gamma}.$$

Here angle $\alpha(0 \leqslant \alpha<2\pi)$ is the angle of rotation about the initial axis z, $\beta(0 \leqslant \beta \leqslant \pi)$ is the angle of rotation about a new (turned) axis y', and $\gamma(0 \leqslant \gamma < 2\pi)$ is one about a new (turned) axis z'. Any rotation of the coordinate system may be performed by successive rotations about coordinate axes z, new y' and new z' at the angles (α,β,γ), respectively. The real functions $d^J_{M_1M_2}(\beta)$ have the following explicit form:

$$d^J_{M_1M_2}(\beta) = (-1)^{M_1-M_2}[(J+M_1)!(J-M_1)!(J+M_2)!(J-M_2)!]^{1/2} \times \sum_k (-1)^k \frac{(\cos\beta/2)^{2J-2k-M_1+M_2}(\sin\beta/2)^{2k+M_1-M_2}}{k!(J-M_1-k)!(J+M_2-k)!(M_1-M_2+k)!}.$$

An index k runs through all the integer values for which the factorial arguments are non-negative, i.e.,

$$\max(0, M_2-M_1) \leq k \leq \min(J-M_1, J+M_2)$$

(cf. [13]). Useful recurrence formulas for computing $d^J_{M_1M_2}(\beta)$ can be found in [12]. In [17] a method for evaluation of $D^J_{M_1M_2}(\alpha,\beta,\gamma)$ for arbitrary arguments from the following relation

$$D^J_{M_1M_2}(\alpha,\beta,\gamma) = \sum_m \mathrm{e}^{-\mathrm{i}M_1\alpha}\, d^J_{M1m}(\pi/2)\, \mathrm{e}^{-\mathrm{i}m\beta}\, d^J_{mM2}(\pi/2)\, \mathrm{e}^{-\mathrm{i}M_2\gamma},$$

is given; the values $d^J_{M1M2}(\pi/2)$ can easily be calculated.

References

[1] S.J. Norton, Tomographic Reconstruction of 2-D vector fields: application to flow imaging, Geophys. J. 97 (1988) 161.
[2] H. Braun, A. Hauck, Tomographic reconstruction of vector fields, IEEE Trans. Signal Process. 39 (2) (1991) 464.

[3] J.L. Prince, Convolution backprojection formulas for 3-d vector tomography with application to MRI, IEEE Trans. Image Process. 5 (10) (1996) 1462.
[4] J.L. Prince, Tomographic reconstruction of 3-D vector fields using inner product probes, IEEE Trans. Image Process. 3 (2) (1994) 216.
[5] P.E. Mijnarends, Determination of anisotropic momentum distribution in positron annihilation, Phys. Rev. B160 (3) (1967) 512.
[6] C.K. Majumdar, Determination of the total momentum distribution by positron annihilation, Phys. Rev. B4 (7) (1971) 2111.
[7] L.M. Pecora, 3D tomographic reconstruction from 2D data using spherical harmonics, IEEE Trans. Nucl. Sci. NS-34 (2) (1987) 642.
[8] L. Wang, R.S. Granetz, Series expansion method in three-dimensional tomography, J. Opt. Soc. Am. A10 (11) (1993) 2292.
[9] S.H. Izen, Inversion of the k-plane transform by orthogonal function series expansion, Inverse Probl. 5 (1989) 181.
[10] L. Wang, The X-ray transform and its inversion for the series expansion basis functions in three-dimensional tomography, SIAM J. Appl. Math. 52 (5) (1992) 1490.
[11] A.L. Balandin, Y. Ono, Tomographic determination of plasma velocity with the use of ion Doppler spectroscopy, Eur. Phys. J. D 17 (2001) 337.
[12] L.C. Biedenharn, J.D. Louck, Angular momentum in quantum physics, Theory and Applications Encyclopedia of Mathematics and its Applications, vol. 8, Addison-Wesley Publishing, 1981.
[13] D.A. Varshalovich, A.N. Moskalev, V.K. Khersonskii, Quantum Theory of Angular Momentum, World Scientific Publishing, 1988.
[14] J.R. Driscoll, D.M. Healy Jr., Computing Fourier Transforms and Convolutions on the 2-Sphere, Adv. Appl. Math. 15 (1994) 202–250.
[15] F. Natterer, The Mathematics of Computerized Tomography, Wiley/B.G. Teubner, Stuttgart, 1986.
[16] P.M. Morse, H. Feshbach, Methods of Theoretical Physics, McGraw-Hill, New York, 1953.
[17] A.R. Edmonds, Angular Momentum in Quantum Mechanics, Princeton University Press, Princeton, NJ, 1960.
[18] Åke Björck, Numerical Methods for Least Squares Problems, SIAM, Philadelphia, 1996.
[19] I.S. Grandshteyn, I.M. Ryzhik, Tables of Integrals, Series and Products, Academic, New York, 1965.
[20] H. Akaike, A new look at the statistical model identification, IEEE Trans. Autom. Control AC-19 (1978) 716.